UNIVERSITYOF BIRMINGHAM

University of Birmingham
Research at Birmingham

Viscoelastic response of carbon fibre reinforced polymer during push-out tests

Corujeira Gallo, Santiago; Li, Xiaoying; Zhang, Zhenxue; Charitidis, Constantinos; Dong, Hanshan

Link to publication on Research at Birmingham portal

Viscoelastic response of carbon fibre reinforced polymer during push-out tests

Santiago CORUJEIRA GALLO [a], Xiaoying LI [a], Zhenxue ZHANG [a], Constantinos

CHARITIDIS [b] and Hanshan DONG [a]

[a] University of Birmingham, School of Metallurgy and Materials

Edgbaston, Birmingham, B15 2TT, United Kingdom.

[b] School of Chemical Engineering, National Technical University of Athens

Iroon Polytechneiou 9, Zografou 157 80, Greece.

*Corresponding author: S. Corujeira Gallo

Phone: +

E-mail: corujeis@bham.ac.uk

Abstract

Push-out is one of the available techniques to assess the bond strength between

the reinforcing fibres and the matrix in composite materials. The test is conducted on

thin sections of composite, and a small indenter is used to apply increasing load on

single fibres while measuring the displacement, until the debonding occurs. This study

used push-out tests to assess the debonding mechanism of carbon fibres in an epoxy

matrix. The tests were conducted at multiple loading rates (0.1 mN/s, 1 mN/s and 10

mN/s) and temperatures (24°C and 125°C). The results were analysed and contrasted

with scanning electron microscopy and atomic force microscopy observations. The data

showed evidence of push-out events and provided new insights into the contribution of

1

the viscoelastic behaviour of the fibre/matrix interface and/or the matrix. This finding could pave new pathways for improving the bond strength between the carbon fibres and the matrix in composite materials.

Keywords: Carbon fibres (A); Polymer-matrix composites (A); Debonding (B); Creep (D)

1. Introduction

Carbon fibre reinforced polymers are composed of two phases: the carbon fibres, which provide strength and stiffness, and the polymeric matrix, which holds the reinforcing fibres in place and distributes the load among individual fibres [1]. The interfacial strength (IFS) between carbon fibres and polymeric matrices has important implications for the mechanical properties of composite materials [2, 3]. In spite of the extensive research efforts, the appropriate assessment of the IFS and its link to the macroscopic properties of composites remains challenging. Several testing methods have been developed to assess the IFS [4], including: micro-bond [5], pull-out [6, 7] or push-out tests [8, 9], fragmentation tests [10, 11] and Raman spectroscopy measurements of specimens under stress [12]. Even though each of these methods can be used to effectively rank the IFS, the results obtained by different methods are not directly comparable [13]. Moreover, it is difficult to link the microscopic test results with the macroscopic properties of composites. The inconsistencies are frequently attributed to the different stress states developed in microscopic and macroscopic conditions [13].

In addition, there is no general agreement on the operating interfacial failure modes. Several models have been proposed with this regard, mainly based on stress and energy failure criteria [9, 14]. However, the limitations of both approaches have been discussed by several authors [15, 16], which could be attributed to the different load-displacement responses of ceramic-matrix and polymer-matrix composites. Clearly, further advance in scientific understanding of the debonding mechanism is important to improve the IFS and to predict the behaviour of composites materials in real operating environments. In this article, the results of push-out tests, conducted at multiple loading rates and temperatures, are presented and discussed. The micro-mechanical tests were supported by microscopic observations to identify the debonding mechanisms.

2. Materials and Methods

2.1. Sample preparation

The samples used for the tests were extracted from a rod of Toray Rebar S12 unidirectional composite, consisting of T700 carbon fibres in an epoxy matrix (Table 1). Discs, 700 µm thick (Figure 1), were extracted from the rod of Rebar S12 using a Struers Accutom 5 precision cut-off machine, fitted with an Al_2O_3 abrasive disc and applying abundant cooling fluid. At least 300 µm of material were removed from each side of the discs by wet grinding with #1200 SiC abrasive paper. Finally, both sides of the discs were ground with #2500 and #4000 SiC abrasive paper and polished for 10 minutes with colloidal silica suspension. In their final condition, the discs had a thickness between 20 µm and 40 µm, which reduces the load needed for the push-out to occur. The samples for the tests were cut from these discs using a sharp scalpel and stored in glass vials under room conditions (20°C and 50% relative humidity).

The glass transition temperature (T_g) of the Rebar S12A was determined using a Mettler Toledo DSC 1 Star calorimeter. Small samples, approximately 14.5 mg in weight, were placed in aluminium pans and heated from room temperature (24°C) to 250°C at a rate of 20°C/min in a nitrogen atmosphere, and subsequently cooled down to room temperature (Figure 2). The first curve obtained in this way was discarded, and the glass transition temperature was determined from the second run, as recommended in Ref. [17].

2.2. Push-out tests

The tests were conducted in a Micro Materials Vantage nanoindentation instrument, fitted with a Berkovich tip and a hot stage. A custom-made holder was manufactured, having 60 µm wide slots produced by electro discharge machining (EDM), where the fibres could be pushed out (Figure 3). The samples were fixed onto the holder using cyanoacrylate adhesive. Individual fibres were selected at random, using an optical microscope with a magnification of 400X. The positioning accuracy of the stage was in the order of 0.5 µm and it was re-calibrated every 8 to 12 tests. The instrument was operated in the displacement-control mode (through a feedback loop with the load) and the loading conditions are listed in Table 2, which consisted of two loading cycles. The first loading cycle was interrupted when the displacement reached 1 µm, which was expected to be close to producing a push-out event, but not sufficient for the Berkovich indenter to contact the surrounding fibres. The load held for 5 s (dwell time at maximum load), and then gradually removed for the fibre and the sample to recover elastically. The second loading cycle was conducted until the displacement reached 2 µm or the load reached 200 mN (whichever condition was reached first). This cycle was expected to reveal information about the friction between the debonded

4

sections of the carbon fibre and the surrounding matrix, as well as to complete the crack propagation thus resulting in a push-out event [15].

During the push-out tests, the temperature of the sample was controlled using a K-type thermocouple embedded in the hot stage of the nano-indentation instrument. The samples were heated up to the target temperature of 125°C, above the T_g of the material, at a rate of 1.6°C/min; the indenter was not actively heated. The temperature was left to stabilise for a minimum of 30 minutes and it was kept constant throughout the test using a temperature controller. The convection losses were minimised using a ceramic wool shielding around the specimen.

The results presented in the article are the average of 16 experiments or the most representative curve of the set. The fitting of the data was conducted with Wolfram Mathematica version 11.3, accounting for the stochastic variation between experiments.

2.3. Characterisation

The specimens were observed in a Jeol 7000 FEG-SEM using a thin carbon coating to improve the conductivity. The observations were only conducted once the tests were finished, so that the damage by the vacuum environment and the localised heating under the electron beam would not affect the results of the push-out tests.

AFM observations were conducted in a Veeco MultiMode SPM, fitted with an AS12 scanner and a silicon nitride cantilever for contact mode. The elastic constant of the selected tip was 0.12 N/m. The results were analysed using the Bruker NanoScope Analysis 1.5 software.

3. Results

3.1. Validity and limitations of the push-out tests

The SEM observations conducted after the push-out tests clearly revealed single

fibres which were pushed-in on the loading side of the samples, i.e. the surface of these

fibres was at a lower plane compared to the nearest neighbours (Figure 4a). The pushed-

in fibres exhibited minimum surface damage, although the edges of the Berkovich

indenter clearly made contact with the surrounding material, causing damage to the

neighbouring fibres. In addition, the observations conducted on the back side of the

samples revealed that the fibres were pushed-out, i.e. the surface of these fibres was at a

higher plane in relation to the surrounding material (Figure 4b).

The AFM observations on the back side of the specimens confirmed that the

fibres were pushed-out (Figure 5). The push-out distance was between 1.0 μm and 1.2

μm in all cases, which is in agreement with the geometrical limitations of the Berkovich

indenter used for the experiments. Once this displacement threshold was reached, the

Berkovich indenter made contact with the surrounding material, thus pushing or

damaging the surrounding fibres. A careful observation of Figure 4 shows the damage

on the surrounding fibres and the displacement of the nearest neighbouring fibres,

relative to the rest of the sample.

Based on these results, it can be concluded that the load-displacement data

obtained during the push-out tests for displacements below the 1.2 μm is representative

of the micro-mechanical response of single fibres in the composite.

3.2. Load-displacement curves

The typical load-displacement curve of the push-out tests is illustrated in Figure 6.

The load and the displacement readings are directly obtained from the nanoindentation

6

instrument, whereas the strain and the stress were calculated using the following

equations:

$$\sigma = \frac{L}{A} = \frac{L}{\pi \varnothing t} \qquad (1)$$

$$\varepsilon = \frac{d}{t} \qquad (2)$$

where σ is the stress, ε is the strain, L is the applied load, A is the average interface area,

$\varnothing$ is the average diameter of the carbon fibres, d is the displacement and t is the

thickness of the specimen.

The characteristic regions of the load-displacement curve are indicated in

Figure 6. The curves typically show a non-linear region at the beginning of the loading

cycle, which finishes at displacements of approximately 200 nm (point 1). This section

of the curve is associated with elastic and plastic deformation of the loaded fibre, until a

conformal contact with the Berkovich indenter is reached. Larger deformations in this

region are typically attributed to the elastic bending of the thin sample between the

supports [18]; the samples exhibiting such behaviour were omitted from this study. The

curve shows a linear region (2), which is attributed to the stiffness of the interface or the

stable crack growth between the carbon fibre and the polymeric matrix. This region

typically finishes at displacements in the order of 650 nm (point 3). At this point, the

displacement increases more rapidly and a departure from the linear trend is observed.

This is attributed to the debonding of the fibre from the matrix or the unstable crack

growth, which often ended with a large displacement at constant load (IFS).

The inset in Figure 6 shows the displacement during the dwell time (region 4).

The increasing deformation at constant load is characteristic of a viscoelastic behaviour

and some push-out events were observed in this region; these events were marked by a

stepwise increase in displacement at constant load. The maximum displacement at the

7

end of this region was invariably in the order 1.2 μm, in agreement with the AFM observations of the fibre displacement after the test. At this point, the load was removed to allow for an elastic recovery and a hysteresis loop was formed upon reloading, which is frequently attributed to energy loses due to friction between the carbon fibre and the polymer [9]. The displacement of the indenter beyond the 1.2 μm threshold is associated with a considerable increase in load, because of the physical contact between the Berkovich indenter and the surrounding fibres.

Table 3 summarises the results of the push-out tests conducted at room temperature and high temperature with different loading rates. In general terms, the samples tested at a low loading rate (0.1 mN/s) showed lower stress values at the characteristic points, compared to the samples tested at 1 mN/s and 10 mN/s; the differences between the latter were negligible. The strain at the characteristic points was comparable for all the loading rate conditions, whereas the loop area (region 5) increased with the loading rate. The results of the tests conducted at high temperature revealed similar trends, although the slope of the linear section (2) was lower, indicating a higher sample compliance at high temperature. In addition, the stress values at characteristic points tended to be lower, but the results were also more scattered. The loop area showed very similar results at room temperature and high temperature, in both cases increasing with the loading rate.

These comments are reflected on the stress and strain curves plotted as a function of time (Figure 7). The stress increased linearly until a maximum point, where the displacement of the fibre reached 1 μm. At this point, the load was held for 5 seconds before unloading. The strain curves show clear signs of residual deformation at the end of the first loading cycle, which are attributed to the pushing-in/out of the carbon fibre

8

under load. The second loading cycle was conducted in a similar way, but in this case the maximum deformation reached 2 μm. It must be mentioned that the displacements beyond 1.2 μm are affected by the interference between the Berkovich indenter and the surrounding material.

The samples tested at high temperature typically required lower loads to reach the 1 μm displacement, defined as the limit for the first loading cycle, thus the total loading time was shorter. The shape of the strain curves at the end of the first loading cycle is noteworthy, where the deflection increases rapidly with minimum changes in the stress or even during the dwell time at constant stress. In addition, some differences can be observed depending on the loading rate and the temperature. The dwell time at maximum load is clearly visible for the high loading rate (10 mN/s), as 5 seconds are a significant portion of the total duration of the experiment. However, the dwell time is relatively short for the experiments conducted at lower loading rates (1 mN/s and 0.1 mN/s) so these curves are presented separately in Figure 8.

The shape of the curves in Figure 8 can be related with the viscoelastic response of the polymeric matrix, which is more evident at high loading rates, in which case the dwell time takes place before the system reaches equilibrium. On the other hand, the response during dwell time is almost linear for the low loading rate (0.1 mN/s), reflecting a system closer to equilibrium. In addition, the viscoelastic response during dwell time is also affected by temperature. The samples tested at high temperature exhibited a much higher compliance compared to the ones tested at room conditions, which is attributed to the different response of the polymer below and above the T_g.

4. Discussion

9

The results presented in the previous section are in agreement with the literature [2, 9, 14-16]. However, the time-dependent response as a function of the loading rate and temperature, as well as the occurrence of push-out events during the dwell time at constant load, are noteworthy (Figure 8a, inset). These phenomena seem to be associated with viscoelastic response of the interface between the carbon fibres and the matrix, or the viscoelastic deformation of the polymer in the immediate vicinity of the tested carbon fibres.

Jäger et al. [16] studied the influence of plastic deformation on the push-out test of carbon fibre reinforced epoxy. The authors observed a deviation in the force-displacement curve from the linear behaviour, which they attributed to plastic deformation as opposed to crack growth. This remark highlights the different response of polymer-matrix and ceramic-matrix composites [9, 14-16]. The time-dependent or viscoelastic deformation is an important mechanism in polymers, which has been reported in nanoindentation experiments [19, 20].

High magnification observations of the pushed-out fibres revealed elongated filaments of polymer still attached to the carbon fibres, even after debonding occurred (Figure 9). The filaments rarely formed in the thin sections of polymer between neighbouring fibres, but they were frequently observed in the isles of polymer between 3 staggered fibres, which resembles the plastic strain simulations in Ref. [16]. These filaments would continue to resist the displacement of the fibre, even at large strains, with the viscoelastic behaviour characteristic of the polymeric matrix.

The viscoelastic response of polymers is often described using a Kelvin-Voigt (Eq. 3) [19, 20] or a logarithmic model (Eq. 4) [21, 22]:

$$\varepsilon(t) = \frac{1}{k}\left(1 - e^{\frac{-t}{\tau}}\right) = \frac{\sigma}{E}\left(1 - e^{\frac{\eta}{E}t}\right) \qquad (3)$$

10

$$\varepsilon(t) = m_{eff} \ln\left(\frac{t}{\Gamma} + 1\right) \tag{4}$$

where ε is the strain, k is the stiffness parameter related with the stress (σ) and the elastic modulus of the interface (E), and τ is the relaxation time constant associated with the viscosity (η) and the elastic modulus (E) and t is the time, m_{eff} is the strain rate sensitivity and Γ is the creep time.

Table 4 shows a summary of the fitting results, which indicate the prevalence of viscoelasticity in the experiments conducted at high loading rates (1 mN/s and 10 mN/s), whereas the samples tested at lower loading rate (0.1 mN/s) exhibited a more linear response during the dwell time. The values also reflect the higher compliance observed in the high temperature experiments, which can be attributed to the softening and drop in stiffness of the polymeric matrix above T_g. The high modulus observed at short time range and low temperature can be attributed to the deformation of the intermolecular distance, which is a high energy distortion mechanism [23]. On the other hand, the reorientation and translation of the chain segments becomes possible at longer times and higher temperatures, and this relaxation is reflected on the decrease in modulus. Unfortunately, the fitting parameters can only be used as figures of merit at this stage, and further work is needed to obtain a detailed molecular interpretation of these values [24].

It is known that physical ageing can have a marked effect on the viscoelastic properties of polymers below T_g [25]. In our case, the samples were stored at room temperature for over 6 months ($> 15 \times 10^6$ seconds), and the duration of the push-out tests was short in comparison (between 10 and 600 seconds). Therefore, the physical ageing during the tests was negligible and the load-displacement-time curves presented in this article are characteristic of a single aged condition (momentary curves) [26].

Mendels et al. [27] reported that the physical ageing of the polymeric matrix had

no significant influence on the IFS in micro-bond tests, and the observed changes were

attributed to variations in internal stresses. Greisel et al. [14] conducted push-out tests

on samples annealed at temperatures above T_g [25], where thermal rejuvenation occurs.

The change in failure mode, from brittle to ductile, was linked with the relaxation of

thermal stresses but the ageing time after annealing was not reported. In view of this,

the effect of physical ageing on the push-out tests may require further study.

The viscoelastic response has interesting implications for the micro-mechanical

models that predict the interaction between the carbon fibres and the polymeric matrix.

In first place, the deviation in the force-displacement curve from the linear behaviour,

which is often associated with debonding, could occur at different stresses depending on

the loading conditions, mainly loading rate, holding time and temperature. This region

dominated by viscoelastic phenomena could be considered an intermediate regime

between the cohesive and frictional regimes [2].

In addition, the contribution made by the friction force between debonded regions

of the carbon fibre and the polymer is likely to be masked by the viscoelastic

components acting on the bonded areas. A separation of these two components would

be difficult, unless a complete debonding of the fibre is achieved. Unfortunately, this

condition was beyond the experimental limitations of the Berkovich indenter used in

this study. The viscoelastic deformation would also take longer time to recover [19],

and this should be taken into account when assessing the dissipative and non-dissipative

mechanisms [16].

Finally, the surface treatment of the carbon fibres may alter the mechanical

properties of the interface material and the thickness of the interface, thus affecting its

12

viscoelastic response. Battisti et al. [28] reported an increase in the interlaminar shear strength when multi-wall carbon nanotubes (MWCNTs) were grafted on the carbon fibres, despite the lack of interaction between the MWCNTs and the carbon fibres. Therefore, it is speculated that the deviation in the force-displacement curve from the linear behaviour observed after some surface treatments could be related with changes in viscoelastic response of the polymer around the fibres, instead of the IFS. This phenomenon could reveal new strengthening and toughening strategies for composite materials [15, 29].

5. Conclusions

The push-out tests conducted on carbon fibre reinforced epoxy using different loading rates and testing temperatures revealed the following conclusions:

- It was possible to push-out single carbon fibres from the matrix with a Berkovich indenter under different loading rates and temperatures (below and above T_g).

- The deviation in the force-displacement curve from the linear behaviour, which is often associated with debonding, could occur at different stresses depending on the loading conditions, mainly loading rate, holding time and temperature.

- The interfacial strength (IFS) and stiffness increased with increasing loading rate and decreased with increasing temperature.

- A time-dependent response was observed in all cases but was more noticeable in the experiments conducted at high loading rate or at high temperature. The behaviour could be described with simple viscoelastic models.

The viscoelastic response has interesting implications for the micro-mechanical models that predict the interaction between the carbon fibres and the polymeric matrix.

13

This phenomenon could reveal new strengthening and toughening strategies for composite materials.

References

[1] Karger-Kocsis J, Mahmood H, Pegoretti A. Recent advances in fiber/matrix interphase engineering for polymer composites. Prog Mater Sci. 2015;73:1-43.

[2] Esqué-de los Ojos D, Ghisleni R, Battisti A, Mohanty G, Michler J, Sort J, et al. Understanding the mechanical behavior of fiber/matrix interfaces during push-in tests by means of finite element simulations and a cohesive zone model. Comp Mater Sci. 2016;117:330-337.

[3] Kabel J, Hosemann P, Zayachuk Y, Armstrong DEJ, Koyanagi T, Katoh Y, et al. Ceramic composites: A review of toughening mechanisms and demonstration of micropillar compression for interface property extraction. J Mater Res. 2018;33(4):424-439.

[4] Zhandarov S, Mäder E. Characterization of fiber/matrix interface strength: Applicability of different tests, approaches and parameters. Compos Sci Technol. 2005;65(1):149-160.

14

[5] Sockalingam S, Nilakantan G. Fiber-matrix interface characterization through the microbond test: A review. Int J Aeronaut Space. 2012;13(3):282-295.

[6] Zhandarov S, Mäder E. Indirect estimation of fiber/polymer bond strength and interfacial friction from maximum load values recorded in the microbond and pull-out tests. Part II: Critical energy release rate. J Adhes Sci Technol. 2003;17(7):967-980.

[7] Zhandarov SF, Mäder E, Yurkevich OR. Indirect estimation of fiber/polymer bond strength and interfacial friction from maximum load values recorded in the microbond and pull-out tests. Part I: Local bond strength. J Adhes Sci Technol. 2002;16(9):1171-1200.

[8] Sha JJ, Dai JX, Li J, Wei ZQ, Hausherr JM, Krenkel W. Measurement and analysis of fiber-matrix interface strength of carbon fiber-reinforced phenolic resin matrix composites. J Compos Mater. 2014;48(11):1303-1311.

[9] Mueller WM, Moosburger-Will J, Sause MGR, Horn S. Microscopic analysis of single-fiber push-out tests on ceramic matrix composites performed with Berkovich and flat-end indenter and evaluation of interfacial fracture toughness. J Eur Ceram Soc. 2013;33(2):441-451.

[10] Andersons J, Joffe R, Hojo M, Ochiai S. Fibre fragment distribution in a single-fibre composite tension test. Compos Part B-Eng. 2001;32(4):323-332.

[11] Huang Y, Young RJ. Analysis of the fragmentation test for carbon-fibre/epoxy model composites by means of Raman spectroscopy. Compos Sci Technol. 1994;52(4):505-517.

15

[12] Paipetis A, Galiotis C. Modelling the stress-transfer efficiency of carbon-epoxy interfaces. P R Soc A. 2001;457(2011):1555-1577.

[13] Pisanova E, Zhandarov S, Mäder E. How can adhesion be determined from micromechanical tests? Compos Part A-Appl S. 2001;32(3-4):425-434.

[14] Greisel M, Jäger J, Moosburger-Will J, Sause MGR, Mueller WM, Horn S. Influence of residual thermal stress in carbon fiber-reinforced thermoplastic composites on interfacial fracture toughness evaluated by cyclic single-fiber push-out tests. Compos Part A-Appl S. 2014;66:117-127.

[15] Mueller WM, Moosburger-Will J, Sause MGR, Greisel M, Horn S. Quantification of crack area in ceramic matrix composites at single-fiber push-out testing and influence of pyrocarbon fiber coating thickness on interfacial fracture toughness. J Eur Ceram Soc. 2015;35(11):2981-2989.

[16] Jäger J, Sause MGR, Burkert F, Moosburger-Will J, Greisel M, Horn S. Influence of plastic deformation on single-fiber push-out tests of carbon fiber reinforced epoxy resin. Compos Part A-Appl S. 2015;71:157-167.

[17] ASTM E1356 Standard Test Method for Assignment of the Glass Transition Temperatures by Differential Scanning Calorimetry; 2014.

[18] Medina CM, Molina-Aldareguía JM, González C, Flores P, Llorca J. Comparison of push-in and push-out tests for measuring interfacial shear strength in nano-reinforced composite materials. J Compos Mater. 2016;50(12):1651-1659.

16

[19] Yang S, Zhang Y-W, Zeng K. Analysis of nanoindentation creep for polymeric

materials. J Appl Phys. 2004;95(7):3655-3666.

[20] Gibson RF. A review of recent research on nanoindentation of polymer composites

and their constituents. Compos Sci Technol. 2014;105:51-65.

[21] Chen J, Bell GA, Dong H, Smith JF, Beake BD. A study of low temperature

mechanical properties and creep behaviour of polypropylene using a new sub-

ambient temperature nanoindentation test platform. J Phys D Appl Phys.

2010;43(42):425404.

[22] Beake BD. Modelling indentation creep of polymers: a phenomenological

approach. J Phys D Appl Phys. 2006;39(20):4478.

[23] Shaw MT, MacKnight WJ. Introduction to polymer viscoelasticity. 3rd ed. USA:

Wiley Interscience; 2005.

[24] Fischer-Cripps AC. A simple phenomenological approach to nanoindentation

creep. Mat Sci Eng A. 2004;385(1):74-82.

[25] Odegard GM, Bandyopadhyay A. Physical aging of epoxy polymers and their

composites. J Polym Sci Pol Phys. 2011;49(24):1695-1716.

[26] Struik LCE. Physical aging in plastics and other glassy materials. Polym Eng Sci.

1977;17(3):165-173.

[27] Mendels D-A, Leterrier Y, Manson J-AE, Nairn JA. The Influence of Internal

Stresses on the Microbond Test II: Physical Aging and Adhesion. J Compos Mater.

2002;36(14):1655-1676.

[28] Battisti A, Esqué-de los Ojos D, Ghisleni R, Brunner AJ. Single fiber push-out

characterization of interfacial properties of hierarchical CNT-carbon fiber

composites prepared by electrophoretic deposition. Compos Sci Technol.

2014;95:121-127.

[29] Moosburger-Will J, Jäger J, Strauch J, Bauer M, Strobl S, Linscheid FF, et al.

Interphase formation and fiber matrix adhesion in carbon fiber reinforced epoxy

resin: influence of carbon fiber surface chemistry. Compos Interface.

2017;24(7):691-710.

Figure captions

Figure 1: Macrographs of the Rebar S12 samples: a) Discs extracted from the rod and b) thin specimen on a spatula, during the final stage of preparation.

Figure 2: Differential scanning calorimetry (DSC) curve of Rebar S12.

Figure 3: Schematic diagram of the experimental set-up used for the push-out tests.

Figure 4: SEM micrographs of a specimen after the push-out tests: a) front side (pushed-in) and b) back side (pushed-out) of the specimen.

Figure 5: AFM observations of a specimen after the push-out test: a) 3D image of the pushed-out fibre and b) cross section profile of the same fibre.

Figure 6: Typical load-displacement curve of the push-out tests. The arrows indicate the loading direction and the inset corresponds to the displacement during the dwell time at constant load (region 4).

Figure 7: Strain-time (solid) and stress-time (dash) curves obtained with different loading rates and temperatures.

Figure 8: Strain-time curves at dwell time (constant load) obtained with different loading rates and temperatures. The graphs show the strain relative to the deformation at the beginning of the dwell time. The fitted exponential (dot line) and logaritmic (dash line) curves are superimposed to the experimental data.

Figure 9: High magnification SEM micrograph of a pushed-out fibre.

19

Tables

Table 1: Nominal mechanical properties of Rebar S12 from specification sheet.

Material	Young's modulus	Tensile strength	Strain at break	Shear strength	Rod diameter	Volume fraction of fibres
Rebar S12	150 GPa	> 1900 MPa	> 1.30%	200 MPa	12 mm	70%

Table 2: Loading conditions used for the push-out tests.

Mode	Number of cycles	Displacement per cycle	Maximum load	Loading rate	Dwell time	Unloading rate
Multiple cycles, depth controlled	2	1 μm	200 mN	0.1 mN/s 1.0 mN/s 10 mN/s	5 s	0.1 mN/s 1.0 mN/s 10 mN/s

Table 3: Summary of results from push-out tests. The reference points correspond to Figure 6.

Loading rate	Stress at point 1 [MPa]	Strain at point 1 [ ]	Slope of linear section 2 [mN / nm]	Stress at point 3 [MPa]	Strain at point 3 [ ]	Maximum stress in Cycle 1 (point 4) [MPa]	Maximum strain in Cycle 1 (point 4) [ ]	Loop area (5) [μJ]
RT 0.1	7.2 ± 1.2	0.007 ± 0.001	35.1 ± 3.5	30.5 ± 3.9	0.021 ± 0.002	39.3 ± 5.4	0.032 ± 0.001	0.80 ± 0.23
RT 1	9.9 ± 1.9	0.009 ± 0.003	39.9 ± 5.4	40.5 ± 6.1	0.025 ± 0.005	53.6 ± 8.0	0.041 ± 0.008	1.30 ± 0.38
RT 10	9.7 ± 1.4	0.008 ± 0.001	40.2 ± 3.9	42.9 ± 1.9	0.023 ± 0.003	52.2 ± 2.7	0.035 ± 0.001	2.84 ± 0.41
HT 0.1	2.8 ± 3.0	0.004 ± 0.004	19.6 ± 4.4	27.2 ± 9.2	0.030 ± 0.005	40.5 ± 12.9	0.054 ± 0.003	0.38 ± 0.14
HT 1	7.3 ± 1.2	0.009 ± 0.002	29.9 ± 3.0	40.9 ± 4.7	0.033 ± 0.005	52.3 ± 4.6	0.050 ± 0.001	1.65 ± 0.22
HT 10	7.4 ± 2.4	0.009 ± 0.002	27.4 ± 4.6	41.9 ± 9.4	0.036 ± 0.006	51.0 ± 8.4	0.048 ± 0.004	2.51 ± 0.86

RT: room temperature (24°C); HT: High temperature (125°C)

22

Table 4: Fitting parameters from Kelvin-Voigt and logarithmic models.

Loading rate	Kelvin-Voigt model				Logarithmic model			
	Room temperature		High temperature		Room temperature		High temperature	
	k	τ	k	τ	m_{eff}	Γ	m_{eff}	Γ
0.1 mN/s	635	3.30	216	6.60	0.09%	1.57	0.33%	4.57
1 mN/s	116	1.50	78	1.45	0.33%	0.23	0.45%	0.29
10 mN/s	80	1.30	70	1.60	0.42%	0.38	0.52%	0.35

Viscoelastic response of carbon fibre reinforced polymer during push-out tests

Santiago CORUJEIRA GALLO [a], Xiaoying LI [a], Zhenxue ZHANG [a], Constantinos

CHARITIDIS [b] and Hanshan DONG [a]

[a] University of Birmingham, School of Metallurgy and Materials

Edgbaston, Birmingham, B15 2TT, United Kingdom.

[b] School of Chemical Engineering, National Technical University of Athens

Iroon Polytechneiou 9, Zografou 157 80, Greece.

*Corresponding author: S. Corujeira Gallo

Phone: +44 (0)121 414 5163

E-mail: corujeis@bham.ac.uk

Abstract

Push-out is one of the available techniques to assess the bond strength between

the reinforcing fibres and the matrix in composite materials. The test is conducted on

thin sections of composite, and a small indenter is used to apply increasing load on

single fibres while measuring the displacement, until the debonding occurs. This study

used push-out tests to assess the debonding mechanism of carbon fibres in an epoxy

matrix. The tests were conducted at multiple loading rates (0.1 mN/s, 1 mN/s and 10

mN/s) and temperatures (24°C and 125°C). The results were analysed and contrasted

with scanning electron microscopy and atomic force microscopy observations. The data

showed evidence of push-out events and provided new insights into the contribution of

1

the viscoelastic behaviour of the fibre/matrix interface and/or the matrix. This finding could pave new pathways for improving the bond strength between the carbon fibres and the matrix in composite materials.

Keywords: Carbon fibres (A); Polymer-matrix composites (A); Debonding (B); Creep (D)

1. Introduction

Carbon fibre reinforced polymers are composed of two phases: the carbon fibres, which provide strength and stiffness, and the polymeric matrix, which holds the reinforcing fibres in place and distributes the load among individual fibres [1]. The interfacial strength (IFS) between carbon fibres and polymeric matrices has important implications for the mechanical properties of composite materials [2, 3]. In spite of the extensive research efforts, the appropriate assessment of the IFS and its link to the macroscopic properties of composites remains challenging. Several testing methods have been developed to assess the IFS [4], including: micro-bond [5], pull-out [6, 7] or push-out tests [8, 9], fragmentation tests [10, 11] and Raman spectroscopy measurements of specimens under stress [12]. Even though each of these methods can be used to effectively rank the IFS, the results obtained by different methods are not directly comparable [13]. Moreover, it is difficult to link the microscopic test results with the macroscopic properties of composites. The inconsistencies are frequently attributed to the different stress states developed in microscopic and macroscopic conditions [13].

In addition, there is no general agreement on the operating interfacial failure modes. Several models have been proposed with this regard, mainly based on stress and energy failure criteria [9, 14]. However, the limitations of both approaches have been discussed by several authors [15, 16], which could be attributed to the different load-displacement responses of ceramic-matrix and polymer-matrix composites. Clearly, further advance in scientific understanding of the debonding mechanism is important to improve the IFS and to predict the behaviour of composites materials in real operating environments. In this article, the results of push-out tests, conducted at multiple loading rates and temperatures, are presented and discussed. The micro-mechanical tests were supported by microscopic observations to identify the debonding mechanisms.

2. Materials and Methods

2.1. Sample preparation

The samples used for the tests were extracted from a rod of Toray Rebar S12 unidirectional composite, consisting of T700 carbon fibres in an epoxy matrix (Table 1). Discs, 700 μm thick (Figure 1), were extracted from the rod of Rebar S12 using a Struers Accutom 5 precision cut-off machine, fitted with an Al_2O_3 abrasive disc and applying abundant cooling fluid. At least 300 μm of material were removed from each side of the discs by wet grinding with #1200 SiC abrasive paper. Finally, both sides of the discs were ground with #2500 and #4000 SiC abrasive paper and polished for 10 minutes with colloidal silica suspension. In their final condition, the discs had a thickness between 20 μm and 40 μm, which reduces the load needed for the push-out to occur. The samples for the tests were cut from these discs using a sharp scalpel and stored in glass vials under room conditions (20°C and 50% relative humidity).

The glass transition temperature (T_g) of the Rebar S12A was determined using a

Mettler Toledo DSC 1 Star calorimeter. Small samples, approximately 14.5 mg in

weight, were placed in aluminium pans and heated from room temperature (24°C) to

250°C at a rate of 20°C/min in a nitrogen atmosphere, and subsequently cooled down to

room temperature (Figure 2). The first curve obtained in this way was discarded, and the

glass transition temperature was determined from the second run, as recommended in

Ref. [17].

2.2. Push-out tests

The tests were conducted in a Micro Materials Vantage nanoindentation

instrument, fitted with a Berkovich tip and a hot stage. A custom-made holder was

manufactured, having 60 µm wide slots produced by electro discharge machining

(EDM), where the fibres could be pushed out (Figure 3). The samples were fixed onto

the holder using cyanoacrylate adhesive. Individual fibres were selected at random,

using an optical microscope with a magnification of 400X. The positioning accuracy of

the stage was in the order of 0.5 μm and it was re-calibrated every 8 to 12 tests. The

instrument was operated in the displacement-control mode (through a feedback loop

with the load) and the loading conditions are listed in Table 2, which consisted of two

loading cycles. The first loading cycle was interrupted when the displacement reached

1 μm, which was expected to be close to producing a push-out event, but not sufficient

for the Berkovich indenter to contact the surrounding fibres. The load held for 5 s

(dwell time at maximum load), and then gradually removed for the fibre and the sample

to recover elastically. The second loading cycle was conducted until the displacement

reached 2 μm or the load reached 200 mN (whichever condition was reached first). This

cycle was expected to reveal information about the friction between the debonded

4

sections of the carbon fibre and the surrounding matrix, as well as to complete the crack propagation thus resulting in a push-out event [15].

During the push-out tests, the temperature of the sample was controlled using a K-type thermocouple embedded in the hot stage of the nano-indentation instrument. The samples were heated up to the target temperature of 125°C, above the T_g of the material, at a rate of 1.6°C/min; the indenter was not actively heated. The temperature was left to stabilise for a minimum of 30 minutes and it was kept constant throughout the test using a temperature controller. The convection losses were minimised using a ceramic wool shielding around the specimen.

The results presented in the article are the average of 16 experiments or the most representative curve of the set. The fitting of the data was conducted with Wolfram Mathematica version 11.3, accounting for the stochastic variation between experiments.

2.3. Characterisation

The specimens were observed in a Jeol 7000 FEG-SEM using a thin carbon coating to improve the conductivity. The observations were only conducted once the tests were finished, so that the damage by the vacuum environment and the localised heating under the electron beam would not affect the results of the push-out tests.

AFM observations were conducted in a Veeco MultiMode SPM, fitted with an AS12 scanner and a silicon nitride cantilever for contact mode. The elastic constant of the selected tip was 0.12 N/m. The results were analysed using the Bruker NanoScope Analysis 1.5 software.

3. Results

3.1. Validity and limitations of the push-out tests

The SEM observations conducted after the push-out tests clearly revealed single

fibres which were pushed-in on the loading side of the samples, i.e. the surface of these

fibres was at a lower plane compared to the nearest neighbours (Figure 4a). The pushed-

in fibres exhibited minimum surface damage, although the edges of the Berkovich

indenter clearly made contact with the surrounding material, causing damage to the

neighbouring fibres. In addition, the observations conducted on the back side of the

samples revealed that the fibres were pushed-out, i.e. the surface of these fibres was at a

higher plane in relation to the surrounding material (Figure 4b).

The AFM observations on the back side of the specimens confirmed that the

fibres were pushed-out (Figure 5). The push-out distance was between 1.0 μm and 1.2

μm in all cases, which is in agreement with the geometrical limitations of the Berkovich

indenter used for the experiments. Once this displacement threshold was reached, the

Berkovich indenter made contact with the surrounding material, thus pushing or

damaging the surrounding fibres. A careful observation of Figure 4 shows the damage

on the surrounding fibres and the displacement of the nearest neighbouring fibres,

relative to the rest of the sample.

Based on these results, it can be concluded that the load-displacement data

obtained during the push-out tests for displacements below the 1.2 μm is representative

of the micro-mechanical response of single fibres in the composite.

3.2. Load-displacement curves

The typical load-displacement curve of the push-out tests is illustrated in Figure 6.

The load and the displacement readings are directly obtained from the nanoindentation

6

instrument, whereas the strain and the stress were calculated using the following

equations:

$$\sigma = \frac{L}{A} = \frac{L}{\pi \, \varnothing \, t} \qquad (1)$$

$$\varepsilon = \frac{d}{t} \qquad (2)$$

where σ is the stress, ε is the strain, L is the applied load, A is the average interface area,

$\varnothing$ is the average diameter of the carbon fibres, d is the displacement and t is the

thickness of the specimen.

The characteristic regions of the load-displacement curve are indicated in

Figure 6. The curves typically show a non-linear region at the beginning of the loading

cycle, which finishes at displacements of approximately 200 nm (point 1). This section

of the curve is associated with elastic and plastic deformation of the loaded fibre, until a

conformal contact with the Berkovich indenter is reached. Larger deformations in this

region are typically attributed to the elastic bending of the thin sample between the

supports [18]; the samples exhibiting such behaviour were omitted from this study. The

curve shows a linear region (2), which is attributed to the stiffness of the interface or the

stable crack growth between the carbon fibre and the polymeric matrix. This region

typically finishes at displacements in the order of 650 nm (point 3). At this point, the

displacement increases more rapidly and a departure from the linear trend is observed.

This is attributed to the debonding of the fibre from the matrix or the unstable crack

growth, which often ended with a large displacement at constant load (IFS).

The inset in Figure 6 shows the displacement during the dwell time (region 4).

The increasing deformation at constant load is characteristic of a viscoelastic behaviour

and some push-out events were observed in this region; these events were marked by a

stepwise increase in displacement at constant load. The maximum displacement at the

end of this region was invariably in the order 1.2 μm, in agreement with the AFM observations of the fibre displacement after the test. At this point, the load was removed to allow for an elastic recovery and a hysteresis loop was formed upon reloading, which is frequently attributed to energy loses due to friction between the carbon fibre and the polymer [9]. The displacement of the indenter beyond the 1.2 μm threshold is associated with a considerable increase in load, because of the physical contact between the Berkovich indenter and the surrounding fibres.

Table 3 summarises the results of the push-out tests conducted at room temperature and high temperature with different loading rates. In general terms, the samples tested at a low loading rate (0.1 mN/s) showed lower stress values at the characteristic points, compared to the samples tested at 1 mN/s and 10 mN/s; the differences between the latter were negligible. The strain at the characteristic points was comparable for all the loading rate conditions, whereas the loop area (region 5) increased with the loading rate. The results of the tests conducted at high temperature revealed similar trends, although the slope of the linear section (2) was lower, indicating a higher sample compliance at high temperature. In addition, the stress values at characteristic points tended to be lower, but the results were also more scattered. The loop area showed very similar results at room temperature and high temperature, in both cases increasing with the loading rate.

These comments are reflected on the stress and strain curves plotted as a function of time (Figure 7). The stress increased linearly until a maximum point, where the displacement of the fibre reached 1 μm. At this point, the load was held for 5 seconds before unloading. The strain curves show clear signs of residual deformation at the end of the first loading cycle, which are attributed to the pushing-in/out of the carbon fibre

8

under load. The second loading cycle was conducted in a similar way, but in this case the maximum deformation reached 2 μm. It must be mentioned that the displacements beyond 1.2 μm are affected by the interference between the Berkovich indenter and the surrounding material.

The samples tested at high temperature typically required lower loads to reach the 1 μm displacement, defined as the limit for the first loading cycle, thus the total loading time was shorter. The shape of the strain curves at the end of the first loading cycle is noteworthy, where the deflection increases rapidly with minimum changes in the stress or even during the dwell time at constant stress. In addition, some differences can be observed depending on the loading rate and the temperature. The dwell time at maximum load is clearly visible for the high loading rate (10 mN/s), as 5 seconds are a significant portion of the total duration of the experiment. However, the dwell time is relatively short for the experiments conducted at lower loading rates (1 mN/s and 0.1 mN/s) so these curves are presented separately in Figure 8.

The shape of the curves in Figure 8 can be related with the viscoelastic response of the polymeric matrix, which is more evident at high loading rates, in which case the dwell time takes place before the system reaches equilibrium. On the other hand, the response during dwell time is almost linear for the low loading rate (0.1 mN/s), reflecting a system closer to equilibrium. In addition, the viscoelastic response during dwell time is also affected by temperature. The samples tested at high temperature exhibited a much higher compliance compared to the ones tested at room conditions, which is attributed to the different response of the polymer below and above the T_g.

4. Discussion

9

The results presented in the previous section are in agreement with the literature [2, 9, 14-16]. However, the time-dependent response as a function of the loading rate and temperature, as well as the occurrence of push-out events during the dwell time at constant load, are noteworthy (Figure 8a, inset). These phenomena seem to be associated with viscoelastic response of the interface between the carbon fibres and the matrix, or the viscoelastic deformation of the polymer in the immediate vicinity of the tested carbon fibres.

Jäger et al. [16] studied the influence of plastic deformation on the push-out test of carbon fibre reinforced epoxy. The authors observed a deviation in the force-displacement curve from the linear behaviour, which they attributed to plastic deformation as opposed to crack growth. This remark highlights the different response of polymer-matrix and ceramic-matrix composites [9, 14-16]. The time-dependent or viscoelastic deformation is an important mechanism in polymers, which has been reported in nanoindentation experiments [19, 20].

High magnification observations of the pushed-out fibres revealed elongated filaments of polymer still attached to the carbon fibres, even after debonding occurred (Figure 9). The filaments rarely formed in the thin sections of polymer between neighbouring fibres, but they were frequently observed in the isles of polymer between 3 staggered fibres, which resembles the plastic strain simulations in Ref. [16]. These filaments would continue to resist the displacement of the fibre, even at large strains, with the viscoelastic behaviour characteristic of the polymeric matrix.

The viscoelastic response of polymers is often described using a Kelvin-Voigt (Eq. 3) [19, 20] or a logarithmic model (Eq. 4) [21, 22]:

$$\varepsilon(t) = \frac{1}{k}\left(1 - e^{\frac{-t}{\tau}}\right) = \frac{\sigma}{E}\left(1 - e^{\frac{\eta}{E}t}\right) \qquad (3)$$

$$\varepsilon(t) = m_{eff} \ln\left(\frac{t}{\Gamma} + 1\right) \tag{4}$$

where ε is the strain, k is the stiffness parameter related with the stress (σ) and the elastic modulus of the interface (E), and τ is the relaxation time constant associated with the viscosity (η) and the elastic modulus (E) and t is the time, m_{eff} is the strain rate sensitivity and Γ is the creep time.

Table 4 shows a summary of the fitting results, which indicate the prevalence of viscoelasticity in the experiments conducted at high loading rates (1 mN/s and 10 mN/s), whereas the samples tested at lower loading rate (0.1 mN/s) exhibited a more linear response during the dwell time. The values also reflect the higher compliance observed in the high temperature experiments, which can be attributed to the softening and drop in stiffness of the polymeric matrix above T_g. The high modulus observed at short time range and low temperature can be attributed to the deformation of the intermolecular distance, which is a high energy distortion mechanism [23]. On the other hand, the reorientation and translation of the chain segments becomes possible at longer times and higher temperatures, and this relaxation is reflected on the decrease in modulus. Unfortunately, the fitting parameters can only be used as figures of merit at this stage, and further work is needed to obtain a detailed molecular interpretation of these values [24].

It is known that physical ageing can have a marked effect on the viscoelastic properties of polymers below T_g [25]. In our case, the samples were stored at room temperature for over 6 months ($> 15 \times 10^6$ seconds), and the duration of the push-out tests was short in comparison (between 10 and 600 seconds). Therefore, the physical ageing during the tests was negligible and the load-displacement-time curves presented in this article are characteristic of a single aged condition (momentary curves) [26].

Mendels et al. [27] reported that the physical ageing of the polymeric matrix had no significant influence on the IFS in micro-bond tests, and the observed changes were attributed to variations in internal stresses. Greisel et al. [14] conducted push-out tests on samples annealed at temperatures above T_g [25], where thermal rejuvenation occurs. The change in failure mode, from brittle to ductile, was linked with the relaxation of thermal stresses but the ageing time after annealing was not reported. In view of this, the effect of physical ageing on the push-out tests may require further study.

The viscoelastic response has interesting implications for the micro-mechanical models that predict the interaction between the carbon fibres and the polymeric matrix. In first place, the deviation in the force-displacement curve from the linear behaviour, which is often associated with debonding, could occur at different stresses depending on the loading conditions, mainly loading rate, holding time and temperature. This region dominated by viscoelastic phenomena could be considered an intermediate regime between the cohesive and frictional regimes [2].

In addition, the contribution made by the friction force between debonded regions of the carbon fibre and the polymer is likely to be masked by the viscoelastic components acting on the bonded areas. A separation of these two components would be difficult, unless a complete debonding of the fibre is achieved. Unfortunately, this condition was beyond the experimental limitations of the Berkovich indenter used in this study. The viscoelastic deformation would also take longer time to recover [19], and this should be taken into account when assessing the dissipative and non-dissipative mechanisms [16].

Finally, the surface treatment of the carbon fibres may alter the mechanical properties of the interface material and the thickness of the interface, thus affecting its

12

viscoelastic response. Battisti et al. [28] reported an increase in the interlaminar shear strength when multi-wall carbon nanotubes (MWCNTs) were grafted on the carbon fibres, despite the lack of interaction between the MWCNTs and the carbon fibres. Therefore, it is speculated that the deviation in the force-displacement curve from the linear behaviour observed after some surface treatments could be related with changes in viscoelastic response of the polymer around the fibres, instead of the IFS. This phenomenon could reveal new strengthening and toughening strategies for composite materials [15, 29].

5. Conclusions

The push-out tests conducted on carbon fibre reinforced epoxy using different loading rates and testing temperatures revealed the following conclusions:

- It was possible to push-out single carbon fibres from the matrix with a Berkovich indenter under different loading rates and temperatures (below and above T_g).

- The deviation in the force-displacement curve from the linear behaviour, which is often associated with debonding, could occur at different stresses depending on the loading conditions, mainly loading rate, holding time and temperature.

- The interfacial strength (IFS) and stiffness increased with increasing loading rate and decreased with increasing temperature.

- A time-dependent response was observed in all cases but was more noticeable in the experiments conducted at high loading rate or at high temperature. The behaviour could be described with simple viscoelastic models.

The viscoelastic response has interesting implications for the micro-mechanical models that predict the interaction between the carbon fibres and the polymeric matrix.

13

This phenomenon could reveal new strengthening and toughening strategies for composite materials.

References

[1] Karger-Kocsis J, Mahmood H, Pegoretti A. Recent advances in fiber/matrix interphase engineering for polymer composites. Prog Mater Sci. 2015;73:1-43.

[2] Esqué-de los Ojos D, Ghisleni R, Battisti A, Mohanty G, Michler J, Sort J, et al. Understanding the mechanical behavior of fiber/matrix interfaces during push-in tests by means of finite element simulations and a cohesive zone model. Comp Mater Sci. 2016;117:330-337.

[3] Kabel J, Hosemann P, Zayachuk Y, Armstrong DEJ, Koyanagi T, Katoh Y, et al. Ceramic composites: A review of toughening mechanisms and demonstration of micropillar compression for interface property extraction. J Mater Res. 2018;33(4):424-439.

[4] Zhandarov S, Mäder E. Characterization of fiber/matrix interface strength: Applicability of different tests, approaches and parameters. Compos Sci Technol. 2005;65(1):149-160.

14

[5] Sockalingam S, Nilakantan G. Fiber-matrix interface characterization through the microbond test: A review. Int J Aeronaut Space. 2012;13(3):282-295.

[6] Zhandarov S, Mäder E. Indirect estimation of fiber/polymer bond strength and interfacial friction from maximum load values recorded in the microbond and pull-out tests. Part II: Critical energy release rate. J Adhes Sci Technol. 2003;17(7):967-980.

[7] Zhandarov SF, Mäder E, Yurkevich OR. Indirect estimation of fiber/polymer bond strength and interfacial friction from maximum load values recorded in the microbond and pull-out tests. Part I: Local bond strength. J Adhes Sci Technol. 2002;16(9):1171-1200.

[8] Sha JJ, Dai JX, Li J, Wei ZQ, Hausherr JM, Krenkel W. Measurement and analysis of fiber-matrix interface strength of carbon fiber-reinforced phenolic resin matrix composites. J Compos Mater. 2014;48(11):1303-1311.

[9] Mueller WM, Moosburger-Will J, Sause MGR, Horn S. Microscopic analysis of single-fiber push-out tests on ceramic matrix composites performed with Berkovich and flat-end indenter and evaluation of interfacial fracture toughness. J Eur Ceram Soc. 2013;33(2):441-451.

[10] Andersons J, Joffe R, Hojo M, Ochiai S. Fibre fragment distribution in a single-fibre composite tension test. Compos Part B-Eng. 2001;32(4):323-332.

[11] Huang Y, Young RJ. Analysis of the fragmentation test for carbon-fibre/epoxy model composites by means of Raman spectroscopy. Compos Sci Technol. 1994;52(4):505-517.

15

[12] Paipetis A, Galiotis C. Modelling the stress-transfer efficiency of carbon-epoxy interfaces. P R Soc A. 2001;457(2011):1555-1577.

[13] Pisanova E, Zhandarov S, Mäder E. How can adhesion be determined from micromechanical tests? Compos Part A-Appl S. 2001;32(3-4):425-434.

[14] Greisel M, Jäger J, Moosburger-Will J, Sause MGR, Mueller WM, Horn S. Influence of residual thermal stress in carbon fiber-reinforced thermoplastic composites on interfacial fracture toughness evaluated by cyclic single-fiber push-out tests. Compos Part A-Appl S. 2014;66:117-127.

[15] Mueller WM, Moosburger-Will J, Sause MGR, Greisel M, Horn S. Quantification of crack area in ceramic matrix composites at single-fiber push-out testing and influence of pyrocarbon fiber coating thickness on interfacial fracture toughness. J Eur Ceram Soc. 2015;35(11):2981-2989.

[16] Jäger J, Sause MGR, Burkert F, Moosburger-Will J, Greisel M, Horn S. Influence of plastic deformation on single-fiber push-out tests of carbon fiber reinforced epoxy resin. Compos Part A-Appl S. 2015;71:157-167.

[17] ASTM E1356 Standard Test Method for Assignment of the Glass Transition Temperatures by Differential Scanning Calorimetry; 2014.

[18] Medina CM, Molina-Aldareguía JM, González C, Flores P, Llorca J. Comparison of push-in and push-out tests for measuring interfacial shear strength in nano-reinforced composite materials. J Compos Mater. 2016;50(12):1651-1659.

[19] Yang S, Zhang Y-W, Zeng K. Analysis of nanoindentation creep for polymeric

materials. J Appl Phys. 2004;95(7):3655-3666.

[20] Gibson RF. A review of recent research on nanoindentation of polymer composites

and their constituents. Compos Sci Technol. 2014;105:51-65.

[21] Chen J, Bell GA, Dong H, Smith JF, Beake BD. A study of low temperature

mechanical properties and creep behaviour of polypropylene using a new sub-

ambient temperature nanoindentation test platform. J Phys D Appl Phys.

2010;43(42):425404.

[22] Beake BD. Modelling indentation creep of polymers: a phenomenological

approach. J Phys D Appl Phys. 2006;39(20):4478.

[23] Shaw MT, MacKnight WJ. Introduction to polymer viscoelasticity. 3rd ed. USA:

Wiley Interscience; 2005.

[24] Fischer-Cripps AC. A simple phenomenological approach to nanoindentation

creep. Mat Sci Eng A. 2004;385(1):74-82.

[25] Odegard GM, Bandyopadhyay A. Physical aging of epoxy polymers and their

composites. J Polym Sci Pol Phys. 2011;49(24):1695-1716.

[26] Struik LCE. Physical aging in plastics and other glassy materials. Polym Eng Sci.

1977;17(3):165-173.

[27] Mendels D-A, Leterrier Y, Manson J-AE, Nairn JA. The Influence of Internal

Stresses on the Microbond Test II: Physical Aging and Adhesion. J Compos Mater.

2002;36(14):1655-1676.

17

[28] Battisti A, Esqué-de los Ojos D, Ghisleni R, Brunner AJ. Single fiber push-out

characterization of interfacial properties of hierarchical CNT-carbon fiber

composites prepared by electrophoretic deposition. Compos Sci Technol.

2014;95:121-127.

[29] Moosburger-Will J, Jäger J, Strauch J, Bauer M, Strobl S, Linscheid FF, et al.

Interphase formation and fiber matrix adhesion in carbon fiber reinforced epoxy

resin: influence of carbon fiber surface chemistry. Compos Interface.

2017;24(7):691-710.

Figure captions

Figure 1: Macrographs of the Rebar S12 samples: a) Discs extracted from the rod and b) thin specimen on a spatula, during the final stage of preparation.

Figure 2: Differential scanning calorimetry (DSC) curve of Rebar S12.

Figure 3: Schematic diagram of the experimental set-up used for the push-out tests.

Figure 4: SEM micrographs of a specimen after the push-out tests: a) front side (pushed-in) and b) back side (pushed-out) of the specimen.

Figure 5: AFM observations of a specimen after the push-out test: a) 3D image of the pushed-out fibre and b) cross section profile of the same fibre.

Figure 6: Typical load-displacement curve of the push-out tests. The arrows indicate the loading direction and the inset corresponds to the displacement during the dwell time at constant load (region 4).

Figure 7: Strain-time (solid) and stress-time (dash) curves obtained with different loading rates and temperatures.

Figure 8: Strain-time curves at dwell time (constant load) obtained with different loading rates and temperatures. The graphs show the strain relative to the deformation at the beginning of the dwell time. The fitted exponential (dot line) and logaritmic (dash line) curves are superimposed to the experimental data.

Figure 9: High magnification SEM micrograph of a pushed-out fibre.

Tables

Table 1: Nominal mechanical properties of Rebar S12 from specification sheet.

Material	Young's modulus	Tensile strength	Strain at break	Shear strength	Rod diameter	Volume fraction of fibres
Rebar S12	150 GPa	> 1900 MPa	> 1.30%	200 MPa	12 mm	70%

Table 2: Loading conditions used for the push-out tests.

Mode	Number of cycles	Displacement per cycle	Maximum load	Loading rate	Dwell time	Unloading rate
Multiple cycles, depth controlled	2	1 μm	200 mN	0.1 mN/s 1.0 mN/s 10 mN/s	5 s	0.1 mN/s 1.0 mN/s 10 mN/s

Table 3: Summary of results from push-out tests. The reference points correspond to Figure 6.

Loading rate	Stress at point 1 [MPa]	Strain at point 1 [ ]	Slope of linear section 2 [mN / nm]	Stress at point 3 [MPa]	Strain at point 3 [ ]	Maximum stress in Cycle 1 (point 4) [MPa]	Maximum strain in Cycle 1 (point 4) [ ]	Loop area (5) [μJ]
RT 0.1	7.2 ± 1.2	0.007 ± 0.001	35.1 ± 3.5	30.5 ± 3.9	0.021 ± 0.002	39.3 ± 5.4	0.032 ± 0.001	0.80 ± 0.23
RT 1	9.9 ± 1.9	0.009 ± 0.003	39.9 ± 5.4	40.5 ± 6.1	0.025 ± 0.005	53.6 ± 8.0	0.041 ± 0.008	1.30 ± 0.38
RT 10	9.7 ± 1.4	0.008 ± 0.001	40.2 ± 3.9	42.9 ± 1.9	0.023 ± 0.003	52.2 ± 2.7	0.035 ± 0.001	2.84 ± 0.41
HT 0.1	2.8 ± 3.0	0.004 ± 0.004	19.6 ± 4.4	27.2 ± 9.2	0.030 ± 0.005	40.5 ± 12.9	0.054 ± 0.003	0.38 ± 0.14
HT 1	7.3 ± 1.2	0.009 ± 0.002	29.9 ± 3.0	40.9 ± 4.7	0.033 ± 0.005	52.3 ± 4.6	0.050 ± 0.001	1.65 ± 0.22
HT 10	7.4 ± 2.4	0.009 ± 0.002	27.4 ± 4.6	41.9 ± 9.4	0.036 ± 0.006	51.0 ± 8.4	0.048 ± 0.004	2.51 ± 0.86

RT: room temperature (24°C); HT: High temperature (125°C)

22

Table 4: Fitting parameters from Kelvin-Voigt and logarithmic models.

Loading rate	Kelvin-Voigt model				Logarithmic model			
	Room temperature		High temperature		Room temperature		High temperature	
	k	τ	k	τ	m_{eff}	$\boldsymbol{\Gamma}$	m_{eff}	$\boldsymbol{\Gamma}$
0.1 mN/s	635	3.30	216	6.60	0.09%	1.57	0.33%	4.57
1 mN/s	116	1.50	78	1.45	0.33%	0.23	0.45%	0.29
10 mN/s	80	1.30	70	1.60	0.42%	0.38	0.52%	0.35

Figure 01
Click here to download high resolution image

a) 10 mm

b) 2 mm
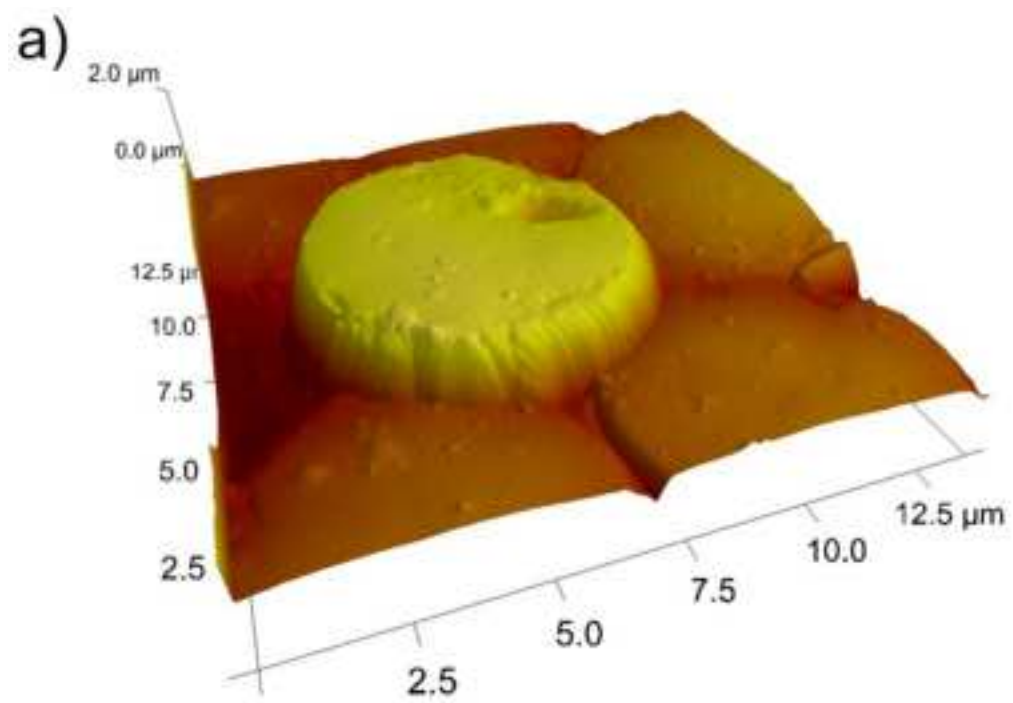
Figure 02
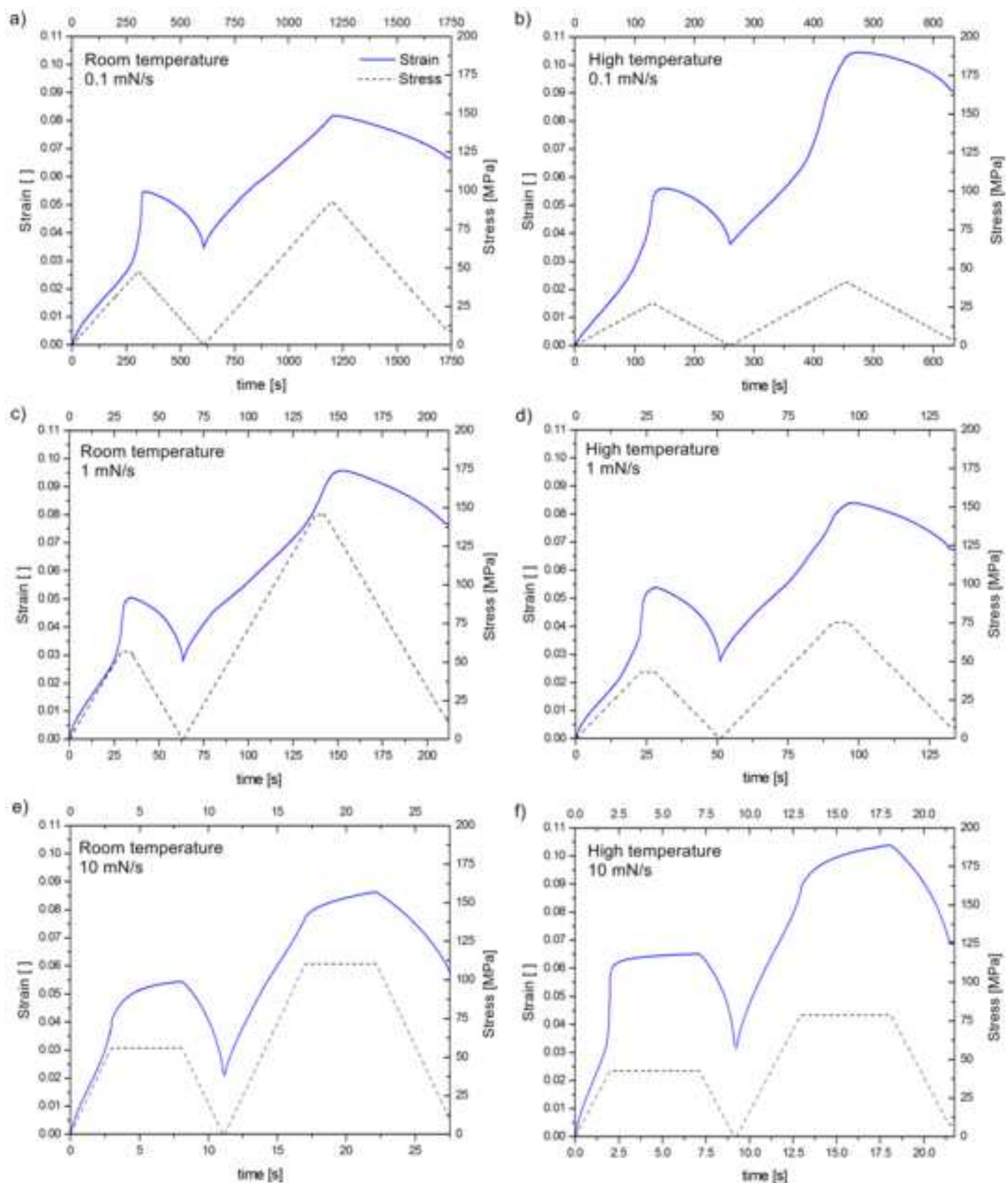
Figure 03
Click here to download high resolution image

Applied force

Berkovich indenter

Thin sample

Fibre

Holder
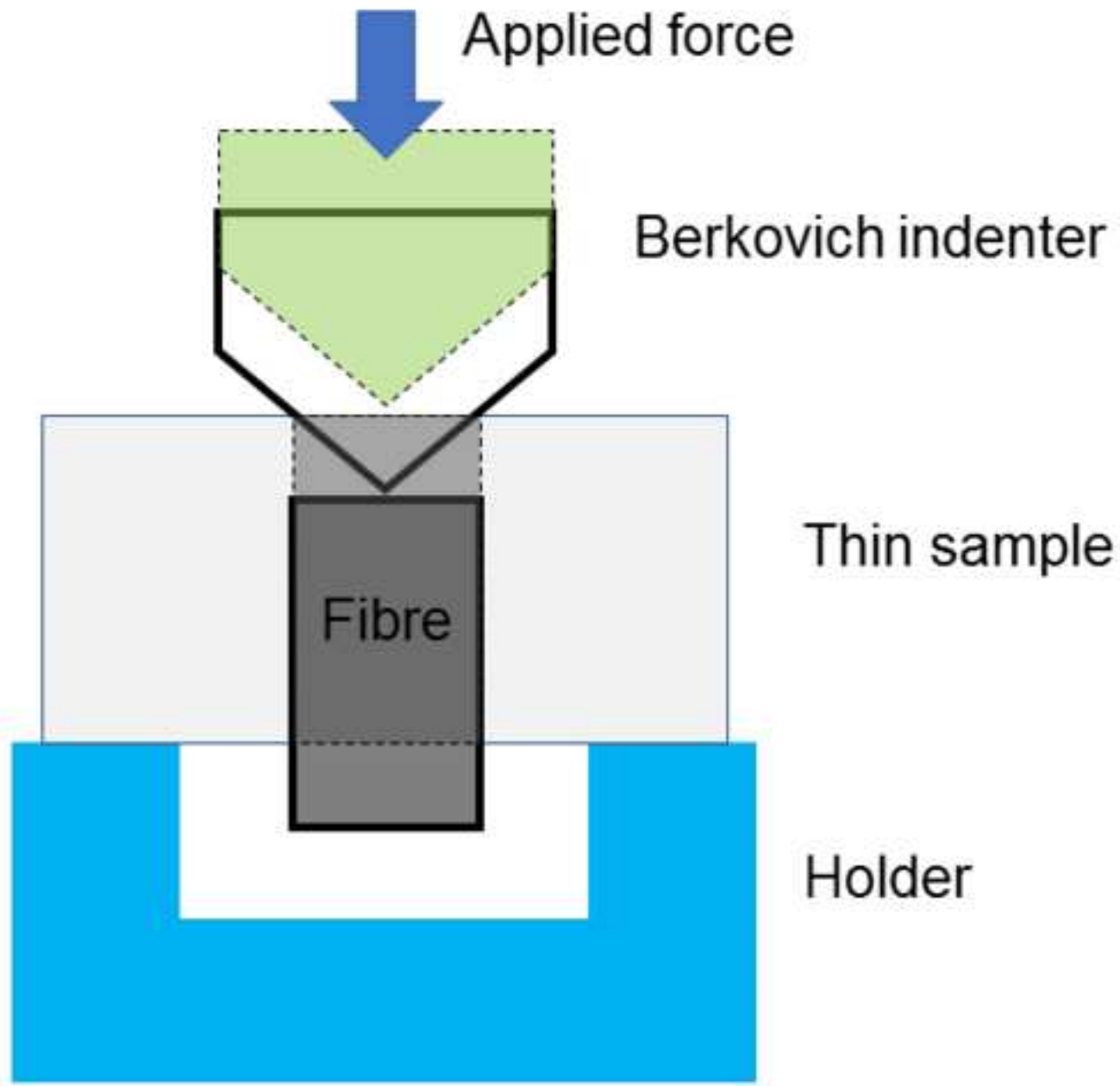
Figure 04
Click here to download high resolution image

a) SEI 20.0kV X5,000 1μm WD 9.4mm

b) SEI 10.1kV X5,000 1μm WD 17.0mm
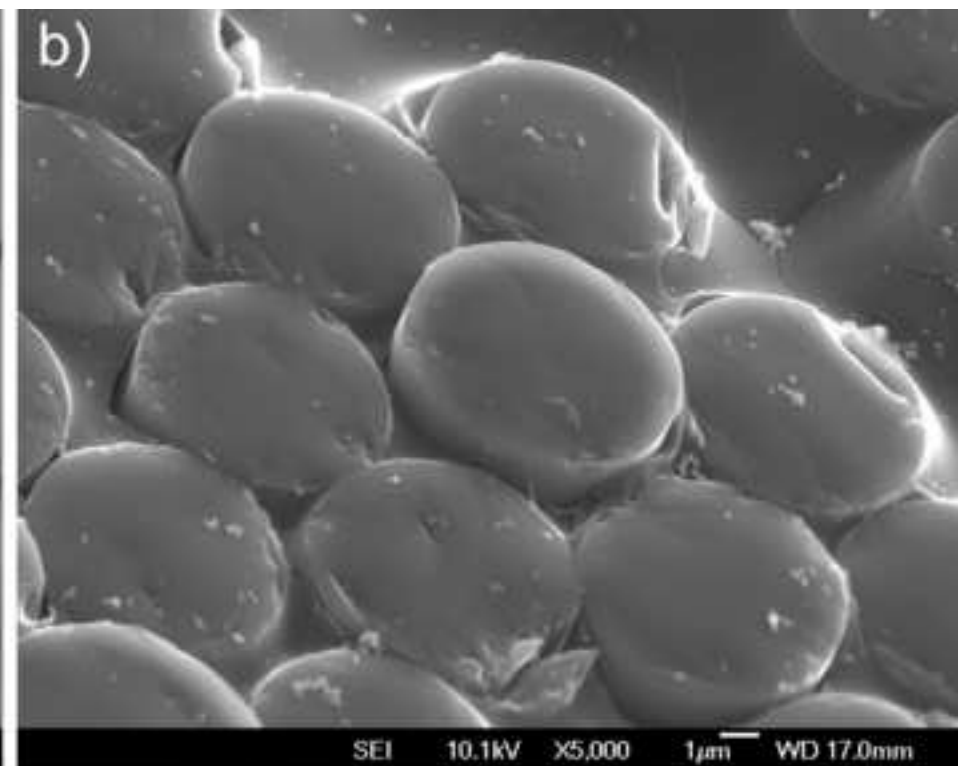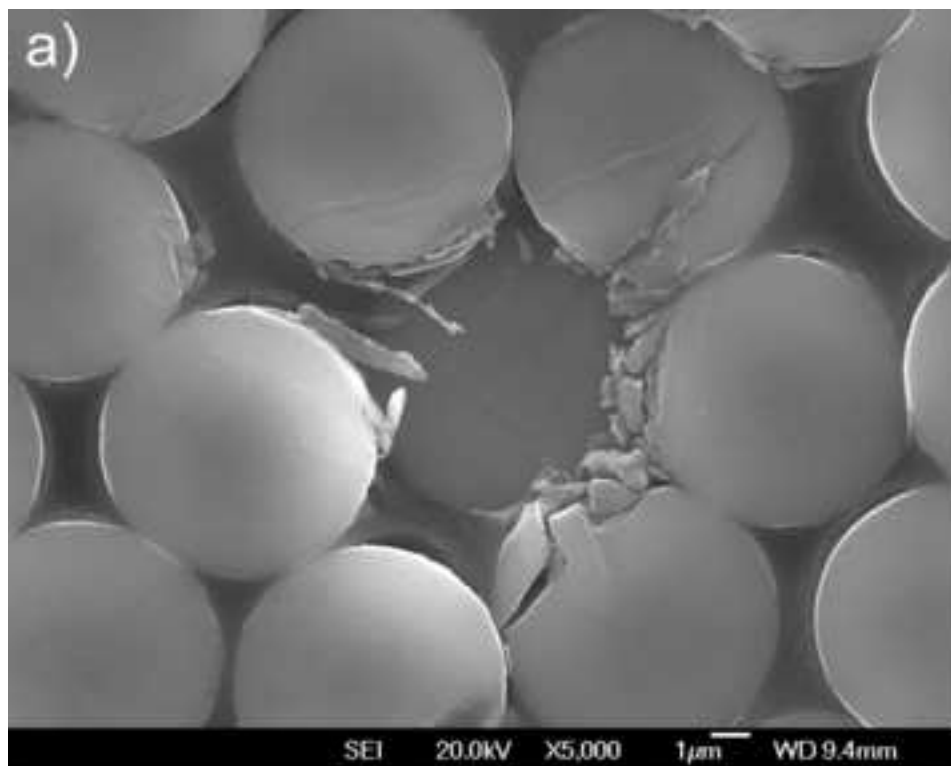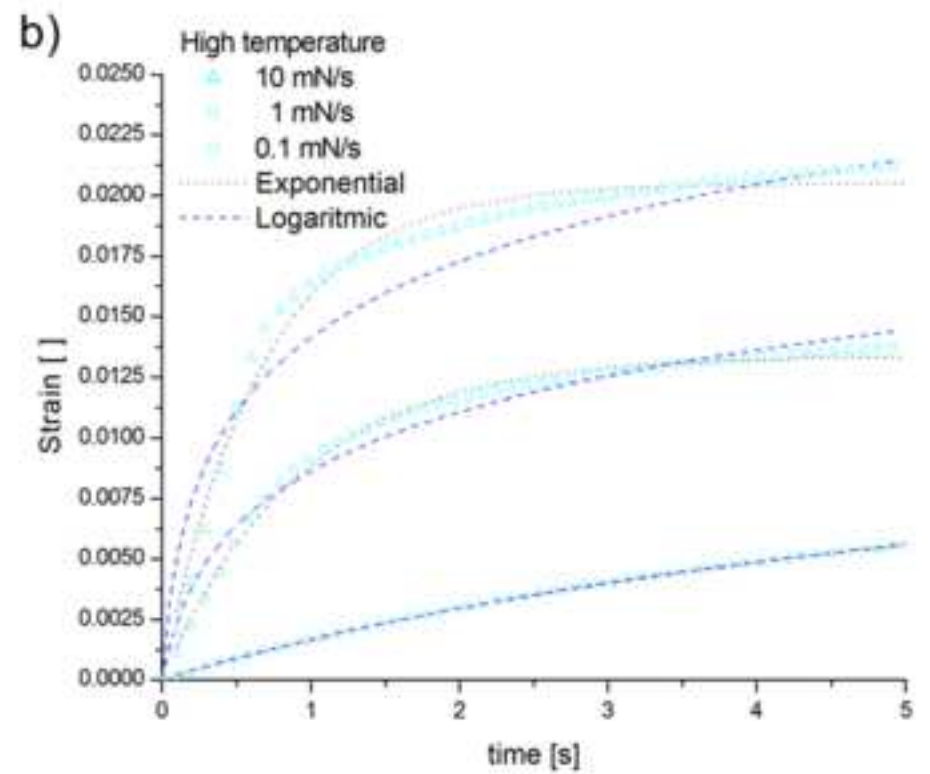
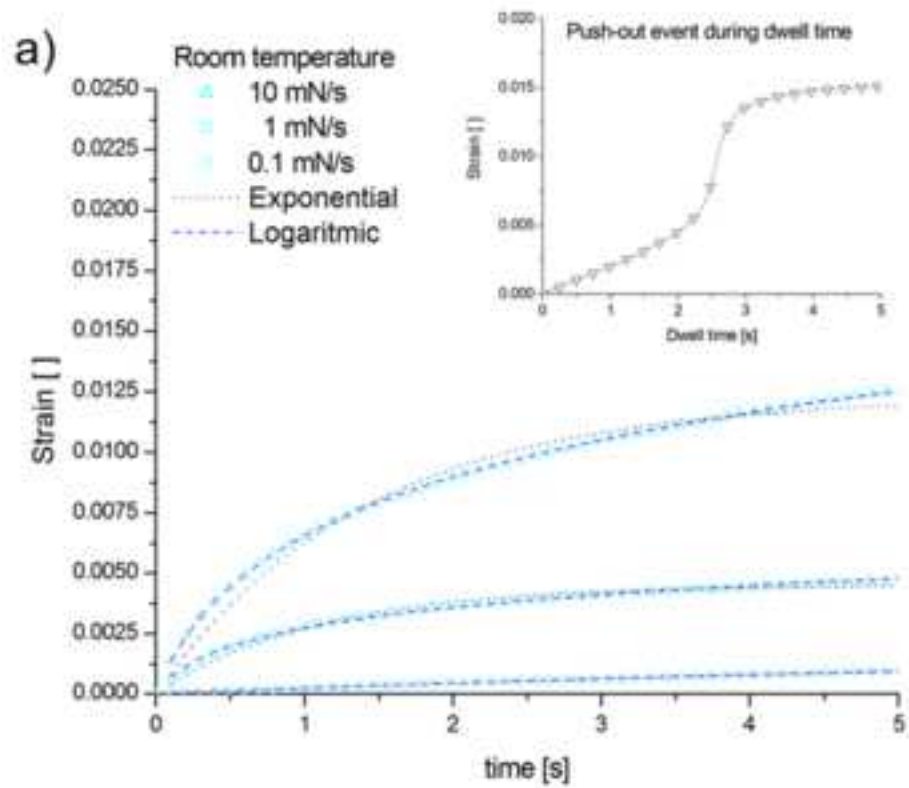**Figure 06**
Click here to download high resolution image
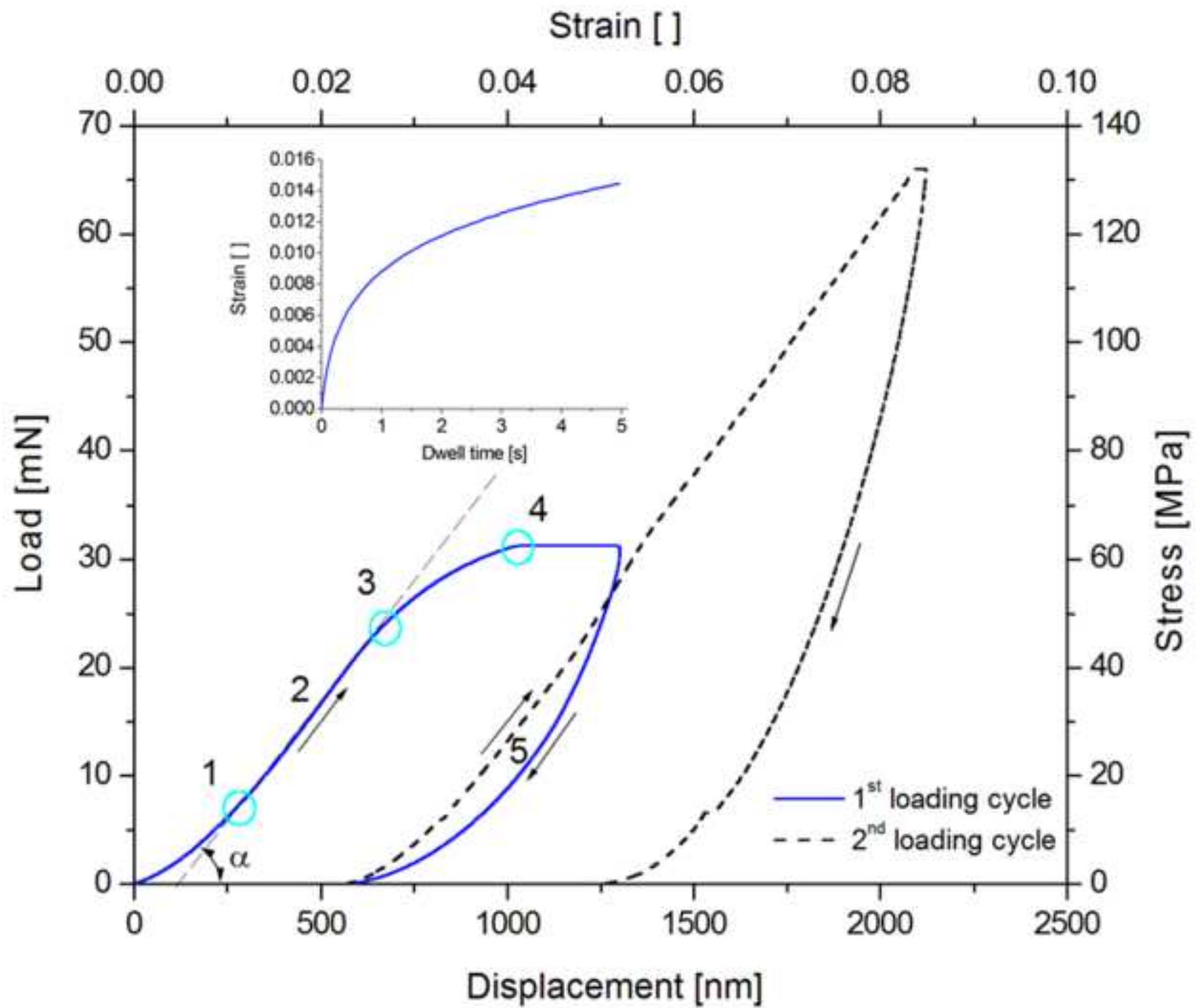
Figure 09
[Click here to download high resolution image](#)